CHIR99021 decreases dopamine content in rat brain striatum through inactivation of Tyrosine Hydroxylase

Sally Hamdon[1,2], Pol Fernandez-Gonzalez[2], Muhammad Yusof Omar[1,2], Jordi Ortiz[1,2,3,4], Carles Gil[1,2,4,5]

[1] Institut de Neurociències, Universitat Autònoma de Barcelona, Spain.

[2] Department of Biochemistry and Molecular Biology, Universitat Autònoma de Barcelona, Spain.

[3] Centro Investigación Biomédica en Red de Salud Mental, CIBERSAM, and Translational Neuroscience Unit, Parc Taulí University Hospital and Universitat Autònoma de Barcelona, Spain.

[4] Contributed equally.

[5]To whom correspondence should be addressed: Carles Gil, Institut de Neurociències and Department of Biochemistry and Molecular Biology, School of Medicine, Room M2-122, Universitat Autònoma de Barcelona, 08193 Bellaterra (Cerdanyola del Vallès, Catalonia), Spain, Tel.: +34 935 81 1524, Fax: +34 93 581 1574, E-mail: carles.gil@uab.cat

Category: Neuropharmacology

Running title: CHIR99021 inhibits TH activity in brain striatum.

ABSTRACT

CHIR99021, also known as laduviglusib or CT99021, is a Glycogen-synthase kinase 3 α/β inhibitor, which has been reported as a promising drug for cardiomyocyte regeneration or treatment of sensorial hearing loss, among other pathologies. Since the activation of dopamine (DA) receptors regulate dopamine synthesis itself and use glycogen-synthase kinase 3β (GSK3β) as an element in the β-arrestin pathway, we decided to check the effect of GSK3β inhibitors (CHIR99021, SB216763 and lithium ion) in the control of DA synthesis. Using *ex vivo* experiments with minces from rat brain striatum, we observed that CHIR99021, but not SB216763 nor lithium, causes a complete abrogation of DA synthesis and accumulation, pointing to off-target effects of CHIR99021. This decrease can be attributed to tyrosine hydroxylase (TH) inhibition since the accumulation of L-DOPA in the presence of a DOPA decarboxylase inhibitor was similarly decreased. On the other hand, CHIR99021 caused an exponential increase in the DOPAC / DA ratio, an indicator of DA metabolization, and decreased the incorporation of extracellular DA into striatum minces. In addition, CHIR99021 or SB216763, but not lithium, decreased TH phosphorylation in Ser19. These results demonstrate that CHIR99021 can lead to TH inactivation and DA decrease in brain striatum, opening the possibility of its use in DA-related disorders, and shows effects to be considered in future clinical trials.

1. INTRODUCTION

Dopamine (DA) transmission is described as essential in the control of behavior through natural rewards, such as food, sex, and nurture, but also by a variety of drugs (Spanagel and Weiss, 1999). Moreover, dysregulation of DA metabolism is a key event in neurodegenerative diseases, such as Parkinson's disease (PD) (Johnson et al., 2018) or in mental disorders, such as schizophrenia (Dahoun et al., 2017). DA acts by neurotransmitter circuits localized in the midbrain, originated in the ventral tegmental area (VTA) and the substantia nigra (SN) and projecting to other brain structures, most prominently the nucleus accumbens shell region, the prefrontal cortex and the striatum (Alcaro et al., 2007). DA levels are the result of its biosynthesis, which is regulated by the first enzyme of the pathway, i.e., Tyrosine hydroxylase (TH; tyrosine 3-monooxygenase; E.C. 1.14.16.2), and of its degradation resulting in 3,4-dihydroxyphenylacetic acid (DOPAC) as its main metabolite. After its synthesis, DA must be internalized into synaptic vesicles by means of the vesicular monoamine transporter 2 (VMAT2) to be released (Meiser et al., 2013). Impairment of the control of these mechanisms may provoke inadequate levels of DA in particular brain areas, which may contribute to behavioral psychiatric pathologies, such as psychosis, addiction (Salamone et al., 2016) or depression (Duda et al., 2020). Moreover, due to the role of DA in the control of coordinated movements, alterations in the dopaminergic system also contribute to diseases causing locomotion impairment (Smith-Dijak et al., 2019). Short-term modulation of TH activity includes phosphorylation (Dunkley et al., 2019) and/or end-product feedback inhibition, i.e., by DA itself (González-Sepúlveda et al., 2022). TH is phosphorylated

at serine residues Ser8, Ser19, Ser31 and Ser40, according to the rat and mouse sequences, while humans show a Thr in position 8. Humans express four TH isoforms (hTH1-4), derived from a single gene, while most species, including rat, express only one isoform (Lewis et al., 1993). Several studies showed that increased phosphorylation at Ser40 positively correlated with TH activity (Bobrovskaya et al. 2007), while phosphorylation of Ser19 and Ser31 increases the rate of phosphorylation of Ser40 and potentiates TH activation (Lehmann et al., 2006).

DA exerts its functions through membrane receptors coupled to G proteins (Thal et al., 2018). DA receptors comprise two classes: the D1-like class (D1 and D5) and the D2-like class (D2, D3 and D4) (Xin et al., 2019). Both classes of receptors can act by two pathways, one inhibits intracellular cAMP via protein G_i (Bonifazi et al., 2019) while the other can initiate a cAMP-independent pathway by promoting a scaffolding complex that leads to the activation of both ERK1/2 and GSK3β signals, through the recruitment of β-arrestin (Jiang et al., 2022). These two pathways are differently turned-on depending on the ligand, in a phenomenon known as biased agonism (Beaulieu & Gainetdinov, 2011). Several evidence link GSK3β with neuropsychiatric disorders, mainly psychosis and schizophrenia (Lovestone et al., 2007; Jope, 2011; Koros and Dorner-Ciossek, 2007; O'Leary and Nolan, 2015). Moreover, inhibition of GSK3β has recently emerged as a possible pharmacological target in a plethora of pathologies, such as hyperglycemia (Ring et al., 2003), lung repair (Uhl et al., 2015), tooth repair (Zaugg et al., 2020), glioblastoma treatment (Oh et al., 2017; Lee et al., 2018) or regeneration of cardiomyocytes (Quaife-Ryan et al., 2020).

A GSK3β inhibitor, CHIR99021 (also known as laduviglusib or CT99021) is currently in clinical phase 2b for the restoration of some types of hearing loss (McLean et al., 2021; ClinicalTrials.gov Identifier: NCT05086276) and is a promising molecule that has also been successfully tested in inhibition of adipogenesis (Bennett et al., 2002), coronary and myocardial diseases (Drakhlis et al., 2021; Badimon et al., 2019), cancer (Oh et al., 2017; Lee et al., 2018; Houben et al., 2022), lung repair therapy (Uhl et al., 2015), stimulation of stem cells (Zhao et al., 2014), and type II diabetes mellitus (Ring et al., 2003). Moreover, CHIR99021 has been proposed as a potential drug for Huntington's disease, acting through off-target effects suppressing the proteasomal degradation of calpastatin (CAST) and enhancing the mitochondrial function (Hu et la., 2021).

In the present work we used *ex vivo* assays with rat brain striatum tissue to study the effects of three GSK3β inhibitors (CHIR99021, SB216763 and lithium) on DA metabolism, since the activation of DA receptors regulate DA synthesis itself and use GSK3β as an element in the β-arrestin pathway. The obtained results demonstrate that CHIR99021 indirectly inhibits TH in brain striatum and should be considered as a potential drug for the treatment of disorders caused by overproduction of DA. The exact mechanism by which CHIR99021 impairs TH activity is still unknown.

2. Materials and methods

2.1. Animals.

Experiments were conducted with male Sprague-Dawley rats weighing 200-250 g (from the Animal Service, Universitat Autònoma de Barcelona or from Charles River). Animals were housed five per cage with ad libitum access to food and water during a 12-hour light/dark cycle. Protocols for animal use were approved by the Ethics Committee for Human and Animal Research (Universitat Autònoma de Barcelona) in accordance with guidelines established by the Ethical Committee for the use of Laboratory Animals in Spain (53/2013) and the European Ethical Committee (2010/63/EU).

2.2. Preparation of striatal minces.

Freshly obtained rat brains were chilled immediately in modified Krebs-Ringer-bicarbonate medium with the following composition: 120 mM NaCl, 0.8 mM KCl, 2.6 mM $CaCl_2$, 0.67 mM $MgSO_4$, 1.2 mM KH_2PO_4, 27.5 mM $NaHCO_3$, and 10 mM glucose, saturated with 95% O_2 / 5% CO_2 and adjusted to pH 7.4. Dorsal / medial striata from both hemispheres were dissected and sliced in a 4°C room using a McIlwain tissue chopper obtaining tissue minces of 0.3 x 0.3 mm / side. Tissue minces were suspended in ice-cold Krebs Ringer bicarbonate medium, and washed three times by centrifugation (1,000 g, 1 min, 4°C), to remove debris of damaged cells, and resuspended. Striatal tissue from a single rat yielded up to 30 aliquots of 25 µL each of the settled minces suspension corresponding to 24 incubation samples and 6 blank samples (0.3 - 0.7 mg protein each). Typically, samples were distributed into 2 mL polypropylene tubes containing 225 µL of ice-cold Krebs Ringer bicarbonate medium. Blank tubes were kept on ice and the rest were incubated at

37°C in soft agitation in an Eppendorf Thermomixer (5 Prime, Inc., Boulder, CO) under 95% O_2 / 5% CO_2 atmosphere.

2.3. Determination of endogenous L-DOPA, DA and DOPAC levels by HPLC-EC.

Levels of L-DOPA, DA and DOPAC were determined in striatal minces. After different incubation times, tissue minces were sonicated in 0.25 M perchloric acid containing 0.25 mM EDTA and 0.1 mM sodium metabisulphite. A 10 µL aliquot was taken for protein quantification by the BCA method (Thermo Fisher Scientific). Samples were spun in an Eppendorf microcentrifuge at 12,000 g for 10 min, and 20 µL of supernatant were used for quantification. The accumulation of L-DOPA in the presence of the decarboxylase inhibitor NSD-1015 100 mM and of DA in the absence of NSD-1015 (Fig. 1B) was quantified by HPLC with coulometric detection (HPLC-EC) as previously described (González-Sepúlveda et al., 2022). The chromatography system consisted of a reverse-phase C18 column (2.5 µm particle Fortis C18, 10 x 0.46 cm, Sugelabor, Spain) and an ion-pair mobile phase, made up of 100 mM sodium phosphate buffer, 1 mM EDTA, 5 mM octanesulfonic acid (pH 2.5) plus 1 % (v/v) methanol. The flow rate was 1 mL / min. Concentrations of L-DOPA, DA and DOPAC were detected with a Coulochem II (ESA) detector with a model 5011 dual-electrode analytical cell with porous graphite electrodes. The potential of electrodes 1 and 2 was set at -0.05 V and +0.4 V respectively. Standards of L-DOPA, DA and DOPAC at different concentrations (4 - 40 nmol) were injected in every experiment to quantify the three metabolites by the external standard method. The obtained concentrations were corrected by protein content in each

sample. Statistical analysis was carried out with GraphPad Prism software (v6, GraphPad Software Inc, USA).

2.4. Newly-synthesized [^{3}H]-DA determination by HPLC-UV.

[^{3}H]-Tyrosine was purified as described previously (González-Sepúlveda et al., 2022). Concentration-response curve of CHIR99021 on striatal [^{3}H]-DA synthesis in minces *ex vivo* was measured after a preincubation period (as in *Preparation of striatal minces* section). CHIR was added using concentrations of 0.3, 3 and 30 µM (n = 6 per concentration) or control without CHIR (n = 6) 10 minutes before the end of preincubation. Then, 0.12 µM purified [^{3}H]-tyrosine was added and incubated for 10 additional minutes. In all experiments, [^{3}H]-DA synthesis was stopped by the addition of 25 µL of a deproteinizing mixture containing trichloroacetic acid (0.5 % w/v), 1 mM ascorbic acid and 25 nmol DA (internal standard). Samples were homogenized in a Dynatech / Sonic Dismembrator (Dynatech Labs, Chantilly, VA). A 10 µL aliquot was taken for protein quantification by the BCA method (Thermo Fisher Scientific). Tissue homogenates were then centrifuged (12,000 g, 10 min, 4°C), and all supernatants were processed for [^{3}H]-DA purification by HPLC-UV. [^{3}H]-DA formed during the incubation reaction was separated from [^{3}H]-tyrosine by HPLC purification by a modification of previous procedures used in our lab for other neurotransmitters (Ortiz et al., 2000). The chromatography system consisted of a reverse-phase C18 column (Tracer Extrasil ODS2, 5 µm particle size, 25 x 0.46 cm; Teknokroma, Spain) and an ion-pair mobile phase, made up of 100 mM sodium phosphate buffer, 1 mM EDTA, 0.75 mM octanesulfonic acid (pH 5) plus 12 % (v/v)

methanol. The flow rate was 1 mL / min. This HPLC system completely separates standards of tyrosine and DA detected by UV 285 nm (ring absorbance). Samples contained extremely low levels of radiolabeled tyrosine and DA that were undetectable by UV absorbance. Similarly, endogenous tyrosine and DA were negligible as compared to the amounts of internal standard DA used. The recovery of the internal standard in each sample (internal / external standard peak area) was quantified from internal standard DA HPLC-UV peak areas. 2 mL fractions corresponding to the DA peak were recovered in scintillation vials, mixed with 6 mL Optiphase HiSafe III cocktail, and quantified in a liquid scintillation counter (Perkin Elmer Tri-Carb 2810TR, USA) to determine [^{3}H]-DA. Disintegrations per minute (dpm) obtained in HPLC-purified [^{3}H]-DA fractions were corrected by DA internal standard recovery and dpm in blank samples. Rate of [^{3}H]-DA synthesis was estimated as the ratio of corrected dpm divided by protein content in each incubate and the incubation time in the presence of [^{3}H]-tyrosine. Results were expressed as a percentage with respect to control samples run in the same experiment.

2.5. Tyrosine Hydroxylase activity in homogenates obtained from striatal striatum.

Striata were extracted and placed in 5-6 mL of cold sodium phosphate buffer 10 mM pH 7.4 and homogenized using a glass Potter homogenizer. 200 µL of homogenates were distributed in incubation tubes in the absence or presence of increasing concentrations of CHIR99021. 100 µM NSD-1015, 30 µM tyrosine and 100 µM tetrahydrobiopterin (BH_4) were added. After 30 min of incubation at 37°C samples were placed in an ice block and 25 µL of a deproteinizing mixture (containing 0.5%

w/v trichloroacetic acid) were added. Samples were centrifuged at 10,000 g for 10 minutes and supernatants are injected into HPLC-ECD to quantify L-DOPA and expressed as L-DOPA pmols / mg protein.

2.6. Western blot.

After incubation of striatal minces as described above, Krebs-Ringer buffer was removed by centrifugation and tissue was homogenized in 1% SDS. Protein amount was determined by BCA. Equal amounts of protein were separated by SDS-PAGE electrophoresis followed by transference in polyvinylidene fluoride membrane in a Trans-Blot Turbo Transfer System (Bio-Rad). Blotting buffer contained 25 mM Tris, 200 mM glycine and 10% methanol (v/v). Membranes were blocked for 1 h with Tris-buffered saline, supplemented with 0.1% Tween 20 and 5% (w/v) defatted powdered milk. Then, the membranes were incubated overnight with the indicated antibody diluted in blocking buffer. The primary antibody from rabbit against β-catenin with triple phosphorylation in the residues Ser33, Ser37 and Thr41 was from Invitrogen (PA5-67518, used at 1:1,000), while the mouse antibody against total β-catenin was from Transduction Laboratories (BD610154, used at 1:1,000). The primary antibodies against TH (AB5280, used at 1:2,500), TH phosphorylated at serine 31 (AB5423, used at 1:1,000) and TH phosphorylated at serine 40 (AB5935, used at 1:1,000) were obtained from Millipore. The antibody against TH phosphorylated at serine 19 (AB5935, used at 1:1,000) was obtained from Thermo Fisher Scientific. The secondary antibodies were IRDye 800CW donkey anti-mouse and IRDye 680RD donkey anti-rabbit (Li-Cor) and were used at 1:10,000 in blocking buffer

supplemented with 0.01% SDS, for 1 h at room temperature in the dark. Infra-red signals were visualized using an Odyssey Fc Infrared Imaging System (Li-Cor). Total and phosphorylated forms were evaluated on the same membrane and the signals were acquired and quantified with Image Studio Lite software. The ratios of phosphorylated to total protein were calculated respect to controls, which were arbitrarily set to 100%.

3. Results.

3.1. CHIR99021 strongly decreases dopamine accumulation and TH activity in rat striatal minces.

Treatment of striatal minces with 3 different concentrations of CHIR99021 yielded a significant decrease in DA accumulation with the two higher concentrations used (3 µM and 30 µM), but not with 0.3 µM, over an incubation period of 2 hours, as determined by HPLC-EC (Figure 1A). The 30 µM concentration was even able to decrease accumulation below the basal level. The IC_{50} of CHIR99021 on DA accumulation was approximately 3 µM. This significant decrease in accumulation was also consistent when minces were incubated for 1, 2 or 4 hours, but not for 30 minutes (Figure 1B). Next, L-DOPA was quantified to assess the effect of CHIR99021 on TH activity. The L-aromatic amino acid decarboxylase that metabolizes L-DOPA was blocked with NSD-1015. Thus, using HPLC-EC we were able to determine that DA synthesis in striatal minces was also significantly reduced in the presence of 0.3 µM, 3 µM and 30 µM CHIR99021 (Figure 1C). To further

investigate the DA metabolism, the levels of DOPAC were also measured, and no significant changes were found at any of the CHIR99021 concentrations tested (Figure 1D), but a dramatic increase in the DOPAC / DA ratio at 30 µM CHIR99021 was detected (Figure 1E). The DOPAC / DA ratio is considered to reflect the degree of DA metabolization by monoamine oxidase (MAO). To determine whether the mentioned effect was due to a direct interaction between CHIR99021 and TH, we also performed the same protocol in homogenates from striatal minces (Figure 1F) and no effect of CHIR99021 was observed. This result suggests that the decrease of L-DOPA levels is not a result from direct interaction of CHIR99021 with TH and therefore the intact intracellular machinery is required.

Since DA accumulation is a result of new DA synthesis and storage, we decided to test its effect on newly synthesized DA using a radioisotopic method to measure [^{3}H]-DA synthesis from [^{3}H]-tyrosine in striatal minces. CHIR99021 decreased [^{3}H]-DA synthesis concentration-dependently (Figure 2A), as in the case of DA accumulation. Western blots against TH were performed, to determine whether the decrease in DA synthesis was due to a decrease in the amount of TH protein. This was not altered after any of the CHIR concentrations tested, either in absolute values or in relation to GAPDH (Figure 2B). Thus, the abrogation of the TH activity by CHIR is not due to loss of TH protein but to a regulatory mechanism affecting efficiency of the enzyme.

3.2. SB216763 and lithium ion do not decrease dopamine content or alter DA metabolization.

To corroborate a role of GSK3β in the decrease of TH activity and DA accumulation, another GSK3β inhibitor such as SB216763 was also tested. SB216763 was able to slightly decrease dopamine accumulation in rat striatal minces over a 2-hour period, but only at 30 µM (Figure 3A) and had no effect at 3 µM or 0.3 µM, even after 4 hours of incubation (Figure 3B). The assessment of TH activity by L-DOPA quantification showed a lack of action by SB216763 at every concentration tested (Figure 3C). Quantification of DOPAC levels at increasing concentrations of SB216763 showed a similar profile than that of DA accumulation shown in 3A, with only a slight decrease of DOPAC amount at 30 µM (Figure 3D), thus yielding a DOPAC / DA ratio unaltered respect to control at any SB216763 concentration (Figure 3E). Given that lithium chloride has antipsychotic properties and has also been reported to inhibit GSK3, the effects of lithium ion on DA metabolism in striatal minces were tested. We observed that 20 mM LiCl yielded a slight but significant decrease in DA accumulation over a 2-hour or 4-hour incubation periods, whereas no effect was detected at 1 or 5 mM (Figure 4A).

3.3. CHIR99021 and SB216763, but not lithium, inhibit GSK3β activity on β-catenin in striatum minces.

GSK3β phosphorylates β-catenin in the residues S33, S37 and T41. Thus, to directly test the inhibitory effect of CHIR99021, SB216763 and of lithium on the GSK3β activity in our system, the amount of triple phosphorylated β-catenin was assessed by western blot. Near infrared-labeled secondary antibodies were used, thus

phosphorylated and total protein levels could be assessed in the same membrane, giving rise to reliable signal quantifications. Treatment with CHIR99021 at 3 µM and with SB216763 at 3 µM for 2h decreased GSK3β-phosphorylated β-catenin by half approximately, whereas lithium at 5 mM for 2h did not show any effect on β-catenin phosphorylation (Figures 5A and 5B). These results corroborate that CHIR99021 and SB216763 cause inhibition of GSK3β in our striatal minces. In consequence, the lack of SB216763 effect on DA metabolism is due to absence of GSK3β action on TH and not to a lack of compound efficiency.

3.4. CHIR99021 and SB216763 decrease TH phosphorylation in serine 19, but not in serines 31 and 40.

Since phosphorylation in serine residues have been described as a regulatory event of TH activity, we explored the effect of CHIR99021 on TH phosphorylation. Western blots with phosphospecific antibodies showed that GSK3β inhibition cause significant decrease of TH phosphorylation in serine 19, approximately 30% after CHIR99021 or SB216763 treatment for 2h (Figure 6A). On the other hand, no changes in phosphorylation were detected neither in serine 31 nor in serine 40 (Figure 6B and 6C). Treatment with LiCl (5 mM for 2h) did not yield change in any of the tested phosphosites (Figure 6A, 6B and 6C).

3.5. CHIR99021 impairs the accumulation of exogenous DA into striatal minces.

To further explore the mechanisms that lead to the dramatic action of CHIR99021 on DA accumulation, we tested the effect of CHIR99021 on DA transport into striatal tissue. Striatal minces were incubated with DA 5 µM in the absence or presence of CHIR99021 30 µM or of tetrabenazine (TBZ) 1 µM, a VMAT2 inhibitor, and the amount of DA incorporated inside tissue was determined by HPLC. Both CHIR99021 and TBZ caused a clear and similar decrease in the amount of DA found inside striatal minces (40% reduction approximately). This result opens the possibility to an effect of CHIR99021 on some component of the DA transport or storage inside cells.

4. Discussion.

GSK3β dysregulation has been described as an event involved in various pathologies, arising as a potential pharmacological target for diseases such as diabetes mellitus, inflammation, tumorigenesis, mental disorders, neurodegenerative diseases or, even, stem cell regeneration (Wada, 2009). CHIR99021 is a small organic molecule that potently inhibits GSK3α (IC_{50}~10 nM) and GSK3β (IC_{50}~5 nM) with high selectivity and is considered the standard activator of the Wnt/β-catenin pathway (Benet et al., 2002). Moreover, it is a compound that has been tested in a plethora of pathologies (Bennett et al., 2002; Drakhlis et al., 2021; Badimon et al., 2019; Oh et al., 2017; Lee et al., 2018; Houben et al., 2022; Uhl et al., 2015; Zhao et al., 2014; Ring et al., 2003), showing pharmacological potential in some of them. Furthermore, treatment of isolated rat pancreatic islets with CHIR99021 or SB216763, another GSK3β inhibitor used in the present work,

increases the rate of beta cell replication (Mussmann et al., 2007). These results point to specific inhibitors of GSK3β as promising tools in diabetes therapies, among others. SB216763 has also been used in retinal stem cell proliferation and maintenance of pluripotent stem cell populations (Inoue et al., 2007). Another GSK3β inhibitor, tideglusib, was tested in clinical trials for Alzheimer's disease, but no clinical benefit was found. Despite that, authors concluded that "further dose finding studies in early disease stages and for longer duration are warranted to examine GSK-3 inhibition in AD patients" (Lovestone et al., 2015). The inhibition of GSK3β as a therapeutical approach is reinforced by the fact that tideglusib has also been proposed as a drug for Amyotrophic Lateral Sclerosis (Martínez-Gonzalez et al., 2021).

Even though CHIR99021 is considered the gold standard for GSK3β inhibition, its off-target effects have been demonstrated. A report describes some action of CHIR99021 on more than 20 kinases as well as the existence of more specific GSK3 inhibitors (An et al., 2012). These off-target effects have been highlighted by a recent report showing that CHIR99021 causes, independently of GSK3, the suppression of the proteasomal degradation of CAST and of the related calpain activity. This leads to a great enhancement of the mitochondrial function by impairing the action of the GTPase dynamin-related protein 1 (Drp1) on mitochondrial fragmentation. The authors hypothesized that CHIR99021 suppresses CAST degradation through inhibition of ubiquitin ligases or activation of deubiquitinases (Hu et al., 2021). Additionally, the promotion by CHIR99021 of mitochondrial biogenesis, oxidative phosphorylation, and the production of reactive oxygen species in human

endodermal progenitor cells have also been observed, in spite that these effects were attributed to the GSK3 / β-catenin pathway and not to off-target effects of CHIR99021 (Ma et al., 2019).

Drp1 has also been involved in regulation of endocytosis and synaptic vesicle recycling, since absence of Drp1 or decrease of its interaction with Bcl-x_L slows endocytosis, produces anormal vesicle membranes and contributes to augmentation of the fast-releasing vesicle pool (Li et al., 2013). Other authors showed that Drp1-defective synapses in *Drosophila* fail to maintain normal neurotransmission, due to the lack of synaptic mitochondria and to defects in the reserve pool vesicles rather than to effects on vesicle recycling (Verstreken et al., 2005). In any case, the action of CHIR99021 on Drp1 could lead to a dysregulation in the synaptic vesicle cycle, altering neurotransmitter uptake and, consequently, affecting the levels of DA in the synaptic terminal and its synthesis pathway.

The feedback inhibition of DA synthesis has previously been described, but the mechanism underlying the process is not clear. Computational analyses have indicated its potential importance in dopaminergic neurotransmission (Wallace, 2007), while *ex vivo* experimental studies have recently revealed that spontaneous inhibition in DA synthesis appeared when storage reached saturation, causing DA spillover and end-product feedback-inhibition of TH in living tissue (González-Sepúlveda et al., 2022). *In vitro* studies suggest the existence in TH of two DA binding sites with high and low affinities (K_D 4 nM and 90 nM, respectively) (Gordon et al., 2008; Nakashima et al., 2009; Dickson and Briggs, 2013; Tekin et al., 2014). The TH low-affinity site / conformation could act as a physiological sensor in case

that synaptic vesicles were filled with DA at its maximum capacity, since the surplus of the DA inside the cytosol of synaptic terminals would bind to the low-affinity site / conformation, causing inhibition of TH activity. This process would happen regardless of the TH phosphorylation status.

Regarding the effect of both CHIR99021 and of SB216763 on TH phosphorylation, Ser19 is reported to be phosphorylated in a 14-3-3 dependent-manner and has little effect on the activity of TH in vitro (Itagaki et al. 1999; Toska et al. 2002). Phosphorylation of TH in Ser19 is related to enzyme degradation of the enzyme by proteasome (Nakashima et al. 2016). The interaction with 14-3-3 proteins, mainly with the γ isoform (Halksau et al., 2009), reduces the sensitivity of phosphorylated human TH isoform 1 to proteolysis by protecting its N-terminal part (Obsilova et al. 2008). Despite the afore mentioned, the dramatic abrogation of TH activity shown in the present work cannot be caused by loss of TH protein, since its levels remain unaltered after CHIR99021 treatment, nor to the relatively small change in phosphoSer19.

One relevant finding of the present work is the dramatic increase of the DOPAC / DA ratio caused by CHIR99021 (Figure 1E). This result can be explained by the enhancement of the MAO activity triggered by the accumulation of its substrate, i.e., DA in the cytosol of the synaptic terminal. This DA accumulation would lead to the inhibition of TH by a feed-back effect, as has been described by our group (González-Sepúlveda et al, 2022) and previously mentioned. An accumulation of DA in striatal minces could also be explained by impairment of the VMAT2 transporter, as has also been observed with TBZ in a previous report from our group (González-

Sepúlveda et al, 2022), giving rise to the possibility that CHIR99021 exerts an off-target inhibitory effect on VMAT2, besides acting as a GSK3β inhibitor. The comparison of the effects of CHIR99021 and TBZ on the transport of extracellular DA inside striatal minces shows a relevant similarity (Figure 7). Since the main portion of the DA in the nerve terminal resides inside synaptic vesicles, where it is protected from metabolism prior to their synaptic release, we can assume that most of the DA incorporated into striatal minces directly reflects the amount of DA inside synaptic vesicles. TBZ is used for the treatment of the motor symptoms in Huntington's disease (HD), a fatal neurodegenerative disorder, and other hyperkinetic disorders (Jankovic, 2009), but it can cause side effects, like nausea, difficulty in speaking, severe muscle stiffness or, even, depression (Jankovic, 2016). In any case, the reduction of DA release in the motor striatum by VMAT2 inhibition is considered a good therapeutic approach to reduce the involuntary hyperkinetic movements of tardive dyskinesia (Stahl, 2018). In fact, CHIR99021 showed to potently improve mitochondrial function and enhance cell viability in several models of HD (Hu et al., 2021). Thus, an available option to TBZ in the hands of the doctors would be a benefit in cases with severe side effects, and CHIR99021 appears as a candidate to be also used in HD or other movement pathologies, such as tardive dyskinesia or Tourette syndrome. Although the exact mechanism of CHIR-mediated TH inhibition has not been fully elucidated, interference with DA storage should be seriously considered.

FIGURE LEGENDS

Figure 1. Effects of CHIR99021 on dopamine accumulation and metabolism in rat brain striatal minces. (A) Concentration-response curve of CHIR99021 in striatal minces *ex vivo*, measuring dopamine (DA) accumulation over an incubation period of 2 hours, using concentrations of 0.3, 3 and 30 μM CHIR99021 or control without CHIR99021 (6 incubates per group obtained from a single animal, n = 6). Basal DA was measured as control samples placed on ice during the 2-hour incubation period (6 incubates, dashed line). **(B)** Time-response curve of DA accumulation in striatal minces *ex vivo* with 3 μM CHIR99021 for 30 minutes, 1 hour, 2 hours, 4 hours (black triangles) and controls (white triangles) for each incubation period. Controls were treated with the corresponding concentration of DMSO used to dissolve CHIR99021 (n = 6), and basal dopamine measured same as in A) and represented as 0 time (n = 6). The same protocol as in A was used in striatal minces to determine L-DOPA **(C)** and DOPAC levels **(D)**. **(E)** The DOPAC / DA ratio was also measured. **(F)** L-DOPA levels after CHIR99021 treatment were measured in homogenates from striatal minces. Data are expressed as mean ± SEM for each group, CHIR99021 vs control, one-way ANOVA followed by Dunnett´s post-hoc test for dose-response graphs and two-way ANOVA followed by Bonferroni's post-hoc test for time-response graph. **$p<0.01$, ***$p<0.001$. Sigmoidal dose-response curve regression was used in every case to create the adjusted curves.

Figure 2. CHIR99021 inhibits tyrosine hydroxylase enzymatic activity. (A) Concentration-response curve of CHIR99021 on striatal [^{3}H]-DA synthesis in minces *ex vivo* was measured after a preincubation period of 2 hours. CHIR99021 was

added using concentrations of 0.3, 3 and 30 μM (n = 6 per concentration) or control without CHIR (n = 6) 10 minutes before the end of preincubation. Then, [^{3}H]-tyrosine was added and incubated for 10 additional minutes. The curve is obtained by normalization of the data to percent of control. In all cases, data are expressed as mean ± SEM for each group. Asterisks indicate **p<0.01 CHIR99021 vs control, one-way ANOVA followed by Dunnett´s post-hoc test. The curve was adjusted to sigmoidal dose-response regression. **(B)** TH amount was assessed by western blot after treatment of minces with 0.3, 3 and 30 μM CHIR99021 or control without CHIR99021 (shown as 0), as in A. GAPDH amount was also detected by western blot and TH / GAPDH ratio was calculated and is represented as a bar graph, which shows means and SEM, after One-way ANOVA analysis with Newman-Keuls post-test, which yielded non-significant in every case. Bands from representative western blots are also shown.

Figure 3. Effect of SB216763 on dopamine accumulation and metabolism in rat brain striatal minces. (A) Concentration-response curve of SB216763, measuring dopamine (DA) accumulation over an incubation period of 2 hours ex vivo, using concentrations of 0.3, 3 and 30 μM SB216763 or control without SB217663 (6 incubates per group obtained from a single animal, n = 6). Basal dopamine was measured as control samples placed on ice during the 2-hour incubation period (6 incubates, dashed line). **(B)** Time-response curve on striatal minces ex vivo for a SB216763 concentration of 3 μM and for 30 minutes, 1 hour, 2 hours, 4 hours, and controls for each incubation period, which were treated with the corresponding concentration of DMSO used to dissolve SB216763 (n = 6), and basal dopamine

measured same as in (A) and represented as 0 time (n = 6). The same protocol as in A was used in striatal minces to determine L-DOPA **(C)** and DOPAC levels **(D)**. **(E)** The DOPAC / DA ratio was also measured. Data are expressed as mean ± SEM for each group, SB216763 vs control, one-way ANOVA followed by Dunnett´s post-hoc test for dose-response graph and two-way ANOVA followed by Bonferroni's post-hoc test for time-response graph. *p<0.5, **p<0.01. Sigmoidal dose-response curve regression was used in every case to create the adjusted curves.

Figure 4. Effect of lithium ion on dopamine accumulation and metabolism in rat brain striatal minces. (A) Concentration-response curve of lithium, measuring DA accumulation over an incubation period of 2 hours *ex vivo*, using concentrations of 1, 5 and 20 mM LiCl or control without lithium (6 incubates per group obtained from a single animal, n = 6). Basal DA was measured as control samples placed on ice during the 2-hour incubation period (6 incubates, dashed line). **(B)** Time-response curve on striatal minces *ex vivo* for a lithium concentration of 20 mM for 30 minutes, 1 hour, 2 hours, 4 hours (n = 6), and basal DA measured same as in (A) and represented as 0 time (n = 6). The same protocol as in A was used in striatal minces to determine L-DOPA **(C)** and DOPAC levels **(D)**. **(E)** The DOPAC / DA ratio was also measured. Data are expressed as mean ± SEM for each group, lithium vs control, one-way ANOVA followed by Dunnett´s post-hoc test for dose-response graph and two-way ANOVA followed by Bonferroni's post-hoc test for time-response graph. *p<0.5, **p<0.01, ***p<0.001. Sigmoidal dose-response curve regression was used in every case to create the adjusted curves.

Figure 5. GSK3β inhibitors CHIR99021 and SB216763, but not lithium, cause decrease in phosphorylation of β-catenin in rat striatal minces. Tissue samples were treated with two GSK3 inhibitors, CHIR99021 (CH, 3 μM) or SB216763 (SB, 3 μM), both for 2h. In parallel, striatal minces were also treated with lithium ion (Li, 5 mM for 2h). Levels of phosho-β-catenin were assessed with western blot using NearIR-labeled secondary antibodies, as described in Materials and Methods section. **A)** Representative western blots are shown after CHIR99021, SB216763 or lithium treatment. Red signal corresponds to β-catenin triple phosphorylated in S33, S37 and T41, green signal corresponds to total β-catenin, while merge of both signals appears in yellow. **B)** Scatter plot representation of the β-catenin phosphorylation ratios (phoshorylated over total) after treatment with CHIR99021, SB216763 or lithium. Each point corresponds to the percentage of the ratio respect to its control, DMSO in the case of CHIR99021 and SB216763 (CD), as vehicle, and water as vehicle in the case of lithium (CW). Graphics shows means ± SEM, after One-way ANOVA analysis with Newman-Keuls post-test. (** $p<0.01$, *** $p<0.001$, n.s. non-significant).

Figure 6. GSK3 inhibitors decrease phosphorylation of Tyrosine Hydroxylase in Ser19, but not in Ser31 or Ser40. Samples from rat striatal minces were treated for 2 hours with CHIR99021 (CH, 3μM), SB216763 (SB, 3μM), lithium chloride (Li, 5mM), DMSO (control for CH99021 and SB216763, shown as CD) and water (control for LiCl, shown as CW). Phosphorylation in every case was assessed by western blot and NIR-labeled secondary antibodies. Red signal corresponds to phosphorylated TH, green signal corresponds to total TH, while merge of both

signals appears in yellow. Representative western blots of phosphorylated TH in Ser19 **(A)**, Ser31 **(B)** and Ser40 **(C)**, after treatment with CHIR99021, SB216763 and lithium ion are shown. Next to each group of western blots, the corresponding Scatter plot representations of every phosphorylation ratio are shown, in every case. Graphics show mean ± SEM, after One-way ANOVA analysis with Newman-Keuls post-test. (*p<0.5, n.s. non-significant).

Figure 7. CHIR99021 decreases dopamine storage inside rat brain striatal minces. When indicated, striatal minces were incubated for 1 h at 37°C with tetrabenazine 1 µM (TBZ), with CHIR99021 30 µM (CHIR) or with Krebs-Ringer buffer (-). For the last 30 min of incubation 5 µM DA was also added in all the three cases. Basal DA was measured as control samples placed on ice during the 1 h incubation period, while Control samples were incubated at 37°C without any drug or DA. Subsequently, minces were recovered by centrifugation and washed once with Krebs-Ringer buffer. The amount of DA incorporated inside tissue was determined in every case by HPLC (pmol DA / mg protein, 6 incubates per group obtained from a single animal). Data are expressed as mean ± SEM for each group. One-way ANOVA test was performed followed by Newman-Keuls post-test, ***p<0.001. Experimental design is shown as a time-line.

CRediT authorship contribution statement

Sally Hamdon: Methodology, Investigation, Formal analysis, Writing - Original Draft, Visualization. **Pol Fernández:** Methodology, Investigation, Formal analysis.

Mohammed Yusof Omar: Methodology, Investigation, Formal analysis. **Jordi Ortiz:** Conceptualization, Validation, Formal analysis, Writing - Original Draft, Visualization, Supervision, Project administration, Funding acquisition. **Carles Gil:** Conceptualization, Validation, Formal analysis, Writing - Original Draft, Visualization, Supervision, Project administration, Funding acquisition.

Declaration of Competing Interest

The authors declare that they have no known competing financial interests or personal relationships that could have appeared to influence the work reported in this paper.

Acknowledgements

This work was supported by Spanish Government grant SAF2017-87199-R. S.H. received a predoctoral fellowship from the Universitat Autònoma de Barcelona. We thank the skillful technical assistance of Susana Benítez

References

Alcaro, A., Huber, R., & Panksepp, J. (2007). Behavioral functions of the mesolimbic dopaminergic system: an affective neuroethological perspective. Brain research reviews, 56(2), 283–321. https://doi.org/10.1016/j.brainresrev.2007.07.014

An WF, Germain AR, Bishop JA, et al. Discovery of Potent and Highly Selective Inhibitors of GSK3β. (2012) In: Probe Reports from the NIH Molecular Libraries

Program [Internet]. Bethesda (MD): National Center for Biotechnology Information (US). https://www.ncbi.nlm.nih.gov/books/NBK133436/

Badimon, L., Casaní, L., Camino-Lopez, S., Juan-Babot, O., & Borrell-Pages, M. (2019). GSK3β inhibition and canonical Wnt signaling in mice hearts after myocardial ischemic damage. PloS one, 14(6), e0218098. https://doi.org/10.1371/journal.pone.0218098

Beaulieu, J. M., & Gainetdinov, R. R. (2011). The physiology, signaling, and pharmacology of dopamine receptors. Pharmacological reviews, 63(1), 182–217. https://doi.org/10.1124/pr.110.002642

Bennett, C. N., Ross, S. E., Longo, K. A., Bajnok, L., Hemati, N., Johnson, K. W., Harrison, S. D., & MacDougald, O. A. (2002). Regulation of Wnt signaling during adipogenesis. The Journal of biological chemistry, 277(34), 30998–31004. https://doi.org/10.1074/jbc.M204527200

Bobrovskaya, L., Gilligan, C., Bolster, E. K., Flaherty, J. J., Dickson, P. W., & Dunkley, P. R. (2007). Sustained phosphorylation of tyrosine hydroxylase at serine 40: a novel mechanism for maintenance of catecholamine synthesis. Journal of neurochemistry, 100(2), 479–489. https://doi.org/10.1111/j.1471-4159.2006.04213.x

Bonifazi, A., Yano, H., Guerrero, A. M., Kumar, V., Hoffman, A. F., Lupica, C. R., Shi, L., & Newman, A. H. (2019). Novel and Potent Dopamine D2 Receptor Go-Protein Biased Agonists. ACS pharmacology & translational science, 2(1), 52–65. https://doi.org/10.1021/acsptsci.8b00060

Dahoun, T., Trossbach, S. V., Brandon, N. J., Korth, C., & Howes, O. D. (2017). The impact of Disrupted-in-Schizophrenia 1 (DISC1) on the dopaminergic system: a systematic review. Translational psychiatry, 7(1), e1015. https://doi.org/10.1038/tp.2016.282

Dickson, P. W., & Briggs, G. D. (2013). Tyrosine hydroxylase: regulation by feedback inhibition and phosphorylation. Advances in pharmacology (San Diego, Calif.), 68, 13–21. https://doi.org/10.1016/B978-0-12-411512-5.00002-6

Drakhlis, L., Devadas, S. B., & Zweigerdt, R. (2021). Generation of heart-forming organoids from human pluripotent stem cells. Nature protocols, 16(12), 5652–5672. https://doi.org/10.1038/s41596-021-00629-8.

Duda, P., Hajka, D., Wójcicka, O., Rakus, D., & Gizak, A. (2020). GSK3β: A Master Player in Depressive Disorder Pathogenesis and Treatment Responsiveness. Cells, 9(3), 727. https://doi.org/10.3390/cells9030727

Dunkley, P. R., & Dickson, P. W. (2019). Tyrosine hydroxylase phosphorylation in vivo. Journal of neurochemistry, 149(6), 706–728. https://doi.org/10.1111/jnc.14675

González-Sepúlveda, M., Omar, M. Y., Hamdon, S., Ma, G., Rosell-Vilar, S., Raivio, N., Abass, D., Martínez-Rivas, A., Vila, M., Giraldo, J., Carrascal, M., Abián, J., Gil, C., Sabriá, J., Ortiz, J., & Moreno-Delgado, D. (2022). Spontaneous changes in brain striatal dopamine synthesis and storage dynamics ex vivo reveal end-product feedback-inhibition of tyrosine hydroxylase. Neuropharmacology, 212, 109058. https://doi.org/10.1016/j.neuropharm.2022.109058

Gordon, S. L., Quinsey, N. S., Dunkley, P. R., & Dickson, P. W. (2008). Tyrosine hydroxylase activity is regulated by two distinct dopamine-binding sites. Journal of neurochemistry, 106(4), 1614–1623. https://doi.org/10.1111/j.1471-4159.2008.05509.x

Halskau, Ø., Jr, Ying, M., Baumann, A., Kleppe, R., Rodriguez-Larrea, D., Almås, B., Haavik, J., & Martínez, A. (2009). Three-way interaction between 14-3-3 proteins, the N-terminal region of tyrosine hydroxylase, and negatively charged membranes. The Journal of biological chemistry, 284(47), 32758–32769. https://doi.org/10.1074/jbc.M109.027706

Houben, R., Hesbacher, S., Sarma, B., Schulte, C., Sarosi, E. M., Popp, S., Adam, C., Kervarrec, T., & Schrama, D. (2022). Inhibition of T-antigen expression promoting glycogen synthase kinase 3 impairs merkel cell carcinoma cell growth. Cancer letters, 524, 259–267. https://doi.org/10.1016/j.canlet.2021.10.031

Hu, D., Sun, X., Magpusao, A., Fedorov, Y., Thompson, M., Wang, B., Lundberg, K., Adams, D. J., & Qi, X. (2021). Small-molecule suppression of calpastatin degradation reduces neuropathology in models of Huntington's disease. Nature communications, 12(1), 5305. https://doi.org/10.1038/s41467-021-25651-y

Inoue, T., Kawaji, T., Inoue-Mochita, M., Taga, T., & Tanihara, H. (2007). Media conditioned by retinal pigment epithelial cells suppress the canonical Wnt pathway. Neuroscience letters, 424(3), 190–193. https://doi.org/10.1016/j.neulet.2007.07.022

Itagaki, C., Isobe, T., Taoka, M., Natsume, T., Nomura, N., Horigome, T., Omata, S., Ichinose, H., Nagatsu, T., Greene, L. A., & Ichimura, T. (1999). Stimulus-coupled interaction of tyrosine hydroxylase with 14-3-3 proteins. Biochemistry, 38(47), 15673–15680. https://doi.org/10.1021/bi9914255

Jankovic J. (2009). Treatment of hyperkinetic movement disorders. The Lancet. Neurology, 8(9), 844-856. https://doi.org/10.1016/S1474-4422(09)70183-8

Jankovic J. (2016). Dopamine depleters in the treatment of hyperkinetic movement disorders. Expert opinion on pharmacotherapy, 17(18), 2461–2470. https://doi.org/10.1080/14656566.2016.1258063

Jiang, H., Galtes, D., Wang, J., & Rockman, H. A. (2022). G protein-coupled receptor signaling: transducers and effectors. American journal of physiology. Cell physiology, 323(3), C731–C748. https://doi.org/10.1152/ajpcell.00210.2022

Johnson, M. E., Salvatore, M. F., Maiolo, S. A., & Bobrovskaya, L. (2018). Tyrosine hydroxylase as a sentinel for central and peripheral tissue responses in Parkinson's progression: Evidence from clinical studies and neurotoxin models. Progress in neurobiology, 165-167, 1–25. https://doi.org/10.1016/j.pneurobio.2018.01.002

Jope R. S. (2011). Glycogen synthase kinase-3 in the etiology and treatment of mood disorders. Frontiers in molecular neuroscience, 4, 16. https://doi.org/10.3389/fnmol.2011.00016

Koros, E., & Dorner-Ciossek, C. (2007). The role of glycogen synthase kinase-3beta in schizophrenia. Drug news & perspectives, 20(7), 437–445. https://doi.org/10.1358/dnp.2007.20.7.1149632

Lee, C., Robinson, M., & Willerth, S. M. (2018). Direct Reprogramming of Glioblastoma Cells into Neurons Using Small Molecules. ACS chemical neuroscience, 9(12), 3175–3185. https://doi.org/10.1021/acschemneuro.8b00365

Lehmann, I. T., Bobrovskaya, L., Gordon, S. L., Dunkley, P. R., & Dickson, P. W. (2006). Differential regulation of the human tyrosine hydroxylase isoforms via hierarchical phosphorylation. Journal of Biological Chemistry, 281(26), 17644-17651. https://doi.org/10.1074/jbc.M512194200

Lewis, D.A, Melchitzky, D.S., Haycock, J.W. (1993). Four isoforms of tyrosine hydroxylase are expressed in human brain. Neuroscience, 54(2) 477-492. https://doi.org/10.1016/0306-4522(93)90267-J.

Li, H., Alavian, K. N., Lazrove, E., Mehta, N., Jones, A., Zhang, P., Licznerski, P., Graham, M., Uo, T., Guo, J., Rahner, C., Duman, R. S., Morrison, R. S., & Jonas, E. A. (2013). A Bcl-xL-Drp1 complex regulates synaptic vesicle membrane dynamics during endocytosis. Nature cell biology, 15(7), 773–785. https://doi.org/10.1038/ncb2791

Lovestone, S., Boada, M., Dubois, B., Hüll, M., Rinne, J. O., Huppertz, H. J., Calero, M., Andrés, M. V., Gómez-Carrillo, B., León, T., del Ser, T., & ARGO investigators (2015). A phase II trial of tideglusib in Alzheimer's disease. Journal of Alzheimer's disease: JAD, 45(1), 75–88. https://doi.org/10.3233/JAD-141959

Lovestone, S., Killick, R., Di Forti, M., & Murray, R. (2007). Schizophrenia as a GSK-3 dysregulation disorder. Trends in neurosciences, 30(4), 142–149. https://doi.org/10.1016/j.tins.2007.02.002

Ma, Y., Ma, M., Sun, J., Li, W., Li, Y., Guo, X., & Zhang, H. (2019). CHIR-99021 regulates mitochondrial remodelling via β-catenin signalling and miRNA expression during endodermal differentiation. Journal of cell science, 132(15), jcs229948. https://doi.org/10.1242/jcs.229948

Martínez-González, L., Gonzalo-Consuegra, C., Gómez-Almería, M., Porras, G., de Lago, E., Martín-Requero, Á., & Martínez, A. (2021). Tideglusib, a Non-ATP

Competitive Inhibitor of GSK-3β as a Drug Candidate for the Treatment of Amyotrophic Lateral Sclerosis. International journal of molecular sciences, 22(16), 8975. https://doi.org/10.3390/ijms2roth2168975

McLean, W. J., Hinton, A. S., Herby, J., Salt, A. N., Hartsock, J. J., Wilson, S., Lucchino, D. L., Lenarz, T., Warnecke, A., Prenzler, N., Schmitt, H., King, S., Jackson, L. E., Rosenbloom, J., Atiee, G., Bear, M., Runge, C. L., Gifford, R. H., Rauch, S. D., Lee, D. J., R. Langer, J.M. Karp, C. Loose, LeBel, C. (2021). Improved Speech Intelligibility in Subjects with Stable Sensorineural Hearing Loss Following Intratympanic Dosing of FX-322 in a Phase 1b Study. Otology & neurotology: official publication of the American Otological Society, American Neurotology Society [and] European Academy of Otology and Neurotology, 42(7), e849–e857. https://doi.org/10.1097/MAO.0000000000003120

Meiser, J., Weindl, D. & Hiller, K. (2013). Complexity of dopamine metabolism. Cell Commun Signal 11, 34 https://doi.org/10.1186/1478-811X-11-34

Mussmann, R., Geese, M., Harder, F., Kegel, S., Andag, U., Lomow, A., Burk, U., Onichtchouk, D., Dohrmann, C., & Austen, M. (2007). Inhibition of GSK3 promotes replication and survival of pancreatic beta cells. The Journal of biological chemistry, 282(16), 12030–12037. https://doi.org/10.1074/jbc.M609637200

Nakashima, A., Hayashi, N., Kaneko, Y. S., Mori, K., Sabban, E. L., Nagatsu, T., & Ota, A. (2009). Role of N-terminus of tyrosine hydroxylase in the biosynthesis of catecholamines. Journal of neural transmission (Vienna, Austria: 1996), 116(11), 1355–1362. https://doi.org/10.1007/s00702-009-0227-8

Nakashima, A., Ohnuma, S., Kodani, Y., Kaneko, Y. S., Nagasaki, H., Nagatsu, T., & Ota, A. (2016). Inhibition of deubiquitinating activity of USP14 decreases tyrosine hydroxylase phosphorylated at Ser19 in PC12D cells. Biochemical and biophysical research communications, 472(4), 598–602. https://doi.org/10.1016/j.bbrc.2016.03.022

Obsilova, V., Nedbalkova, E., Silhan, J., Boura, E., Herman, P., Vecer, J., Sulc, M., Teisinger, J., Dyda, F., & Obsil, T. (2008). The 14-3-3 protein affects the conformation of the regulatory domain of human tyrosine hydroxylase. Biochemistry, 47(6), 1768–1777. https://doi.org/10.1021/bi7019468

Oh, J., Kim, Y., Che, L., Kim, J. B., Chang, G. E., Cheong, E., Kang, S. G., & Ha, Y. (2017). Regulation of cAMP and GSK3 signaling pathways contributes to the neuronal conversion of glioma. PloS one, 12(11), e0178881. https://doi.org/10.1371/journal.pone.0178881

O'Leary, O., & Nolan, Y. (2015). Glycogen synthase kinase-3 as a therapeutic target for cognitive dysfunction in neuropsychiatric disorders. CNS drugs, 29(1), 1–15. https://doi.org/10.1007/s40263-014-0213-z

Ortiz, J., Gómez, J., Torrent, A., Aldavert, M., & Blanco, I. (2000). Quantitative radioisotopic determination of histidine decarboxylase using high-performance liquid chromatography. Analytical biochemistry, 280(1), 111–117. https://doi.org/10.1006/abio.2000.4494

Quaife-Ryan, G. A., Mills, R. J., Lavers, G., Voges, H. K., Vivien, C. J., Elliott, D. A., Ramialison, M., Hudson, J. E., & Porrello, E. R. (2020). β-Catenin drives distinct transcriptional networks in proliferative and nonproliferative cardiomyocytes. Development (Cambridge, England), 147(22), dev193417. https://doi.org/10.1242/dev.193417

Ring, D. B., Johnson, K. W., Henriksen, E. J., Nuss, J. M., Goff, D., Kinnick, T. R., Ma, S. T., Reeder, J. W., Samuels, I., Slabiak, T., Wagman, A. S., Hammond, M. E., & Harrison, S. D. (2003). Selective glycogen synthase kinase 3 inhibitors potentiate insulin activation of glucose transport and utilization in vitro and in vivo. Diabetes, 52(3), 588–595. https://doi.org/10.2337/diabetes.52.3.588

Salamone, J. D., Yohn, S. E., López-Cruz, L., San Miguel, N., & Correa, M. (2016). Activational and effort-related aspects of motivation: neural mechanisms and implications for psychopathology. Brain: a journal of neurology, 139(Pt 5), 1325–1347. https://doi.org/10.1093/brain/aww050

Smith-Dijak, A. I., Sepers, M. D., & Raymond, L. A. (2019). Alterations in synaptic function and plasticity in Huntington disease. Journal of neurochemistry, 150(4), 346–365. https://doi.org/10.1111/jnc.14723

Spanagel, R., & Weiss, F. (1999). The dopamine hypothesis of reward: past and current status. Trends in neurosciences, 22(11), 521–527. https://doi.org/10.1016/s0166-2236(99)01447-2

Stahl, S. (2018). Mechanism of action of vesicular monoamine transporter 2 (VMAT2) inhibitors in tardive dyskinesia: Reducing dopamine leads to less “go” and more “stop” from the motor striatum for robust therapeutic effects. CNS Spectrums, 23(1), 1-6. doi:10.1017/S1092852917000621

Tekin, I., Roskoski, R., Jr, Carkaci-Salli, N., & Vrana, K. E. (2014). Complex molecular regulation of tyrosine hydroxylase. Journal of neural transmission (Vienna, Austria: 1996), 121(12), 1451–1481. https://doi.org/10.1007/s00702-014-1238-7

Thal, D. M., Glukhova, A., Sexton, P. M., & Christopoulos, A. (2018). Structural insights into G-protein-coupled receptor allostery. Nature, 559(7712), 45–53. https://doi.org/10.1038/s41586-018-0259-z

Toska, K., Kleppe, R., Armstrong, C. G., Morrice, N. A., Cohen, P., & Haavik, J. (2002). Regulation of tyrosine hydroxylase by stress-activated protein kinases. Journal of neurochemistry, 83(4), 775–783. https://doi.org/10.1046/j.1471-4159.2002.01172.x

Uhl, F. E., Vierkotten, S., Wagner, D. E., Burgstaller, G., Costa, R., Koch, I., Lindner, M., Meiners, S., Eickelberg, O., & Königshoff, M. (2015). Preclinical validation and imaging of Wnt-induced repair in human 3D lung tissue cultures. The European respiratory journal, 46(4), 1150–1166. https://doi.org/10.1183/09031936.00183214

Verstreken, P., Ly, C. V., Venken, K. J., Koh, T. W., Zhou, Y., & Bellen, H. J. (2005). Synaptic mitochondria are critical for mobilization of reserve pool vesicles at Drosophila neuromuscular junctions. Neuron, 47(3), 365–378. https://doi.org/10.1016/j.neuron.2005.06.018

Wada A. (2009). GSK-3 inhibitors and insulin receptor signaling in health, disease, and therapeutics. Frontiers in bioscience (Landmark edition), 14(4), 1558–1570. https://doi.org/10.2741/3324

Wallace L. J. (2007). A small dopamine permeability of storage vesicle membranes and end product inhibition of tyrosine hydroxylase are sufficient to explain changes occurring in dopamine synthesis and storage after inhibition of neuron firing. Synapse (New York, N.Y.), 61(9), 715–723. https://doi.org/10.1002/syn.20408

Xin, J., Fan, T., Guo, P., & Wang, J. (2019). Identification of functional divergence sites in dopamine receptors of vertebrates. Computational biology and chemistry, 83, 107140. https://doi.org/10.1016/j.compbiolchem.2019.107140

Zaugg, L. K., Banu, A., Walther, A. R., Chandrasekaran, D., Babb, R. C., Salzlechner, C., Hedegaard, M., Gentleman, E., & Sharpe, P. T. (2020). Translation Approach for Dentine Regeneration Using GSK-3 Antagonists. Journal of dental research, 99(5), 544–551. https://doi.org/10.1177/0022034520908593

Zhao, J., Li, S., Trilok, S., Tanaka, M., Jokubaitis-Jameson, V., Wang, B., Niwa, H., & Nakayama, N. (2014). Small molecule-directed specification of sclerotome-like chondroprogenitors and induction of a somatic chondrogenesis program from embryonic stem cells. Development (Cambridge, England), 141(20), 3848–3858. https://doi.org/10.1242/dev.105981

Figure 1

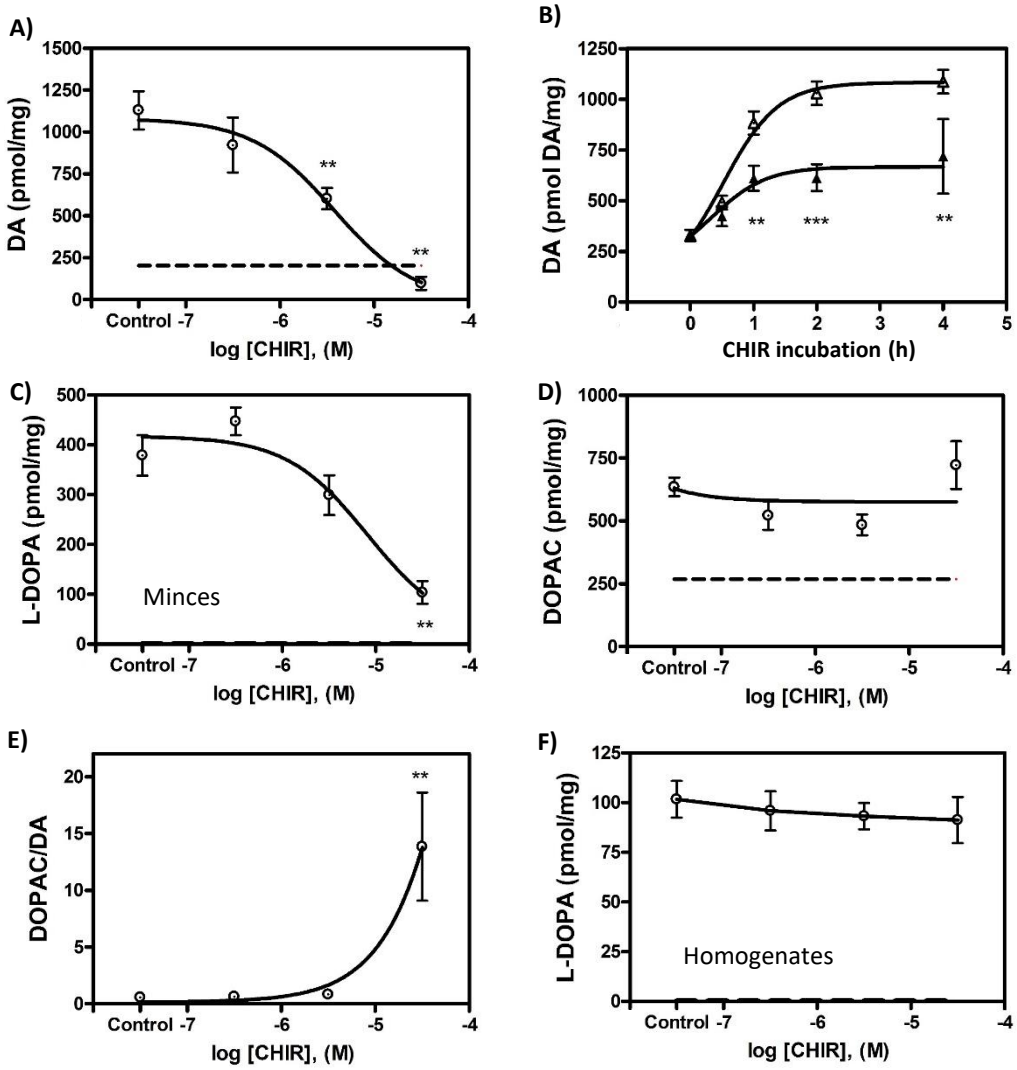
A)
DA (pmol/mg)
1500
1250
1000
750
500
250
0
**
**
Control -7
-6
-5
-4
log [CHIR], (M)
B)
DA (pmol DA/mg)
1250
1000
750
500
250
0
**
***
**
0
1
2
3
4
5
CHIR incubation (h)
C)
L-DOPA (pmol/mg)
500
400
300
200
100
0
Minces
**
Control -7
-6
-5
-4
log [CHIR], (M)
D)
DOPAC (pmol/mg)
1000
750
500
250
0
Control -7
-6
-5
-4
log [CHIR], (M)
E)
DOPAC/DA
20
15
10
5
0
**
Control -7
-6
-5
-4
log [CHIR], (M)
F)
L-DOPA (pmol/mg)
125
100
75
50
25
0
Homogenates
Control -7
-6
-5
-4
log [CHIR], (M)

Figure 2

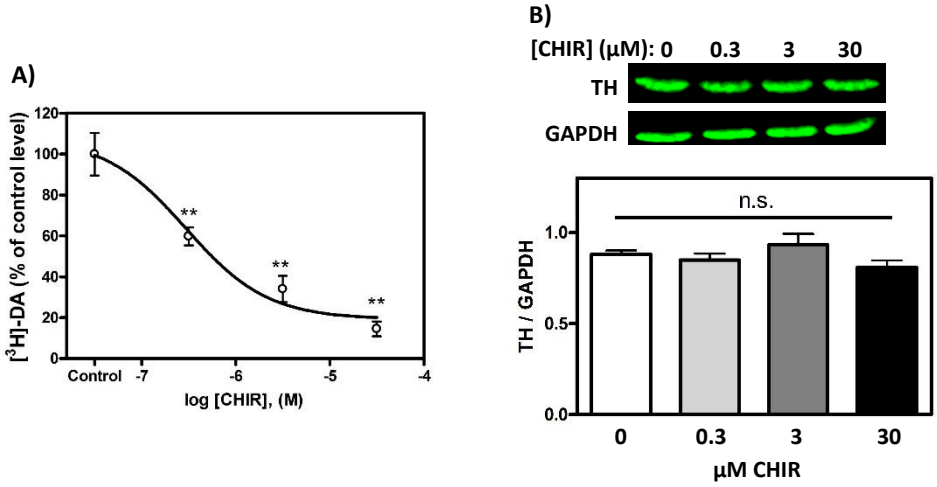
A)
[3H]-DA (% of control level)
120
100
80
60
40
20
0
**
**
**
Control
-7
-6
-5
-4
log [CHIR], (M)
B)
[CHIR] (μM): 0 0.3 3 30
TH
GAPDH
n.s.
TH / GAPDH
1.0
0.5
0.0
0
0.3
3
30
μM CHIR

Figure 3

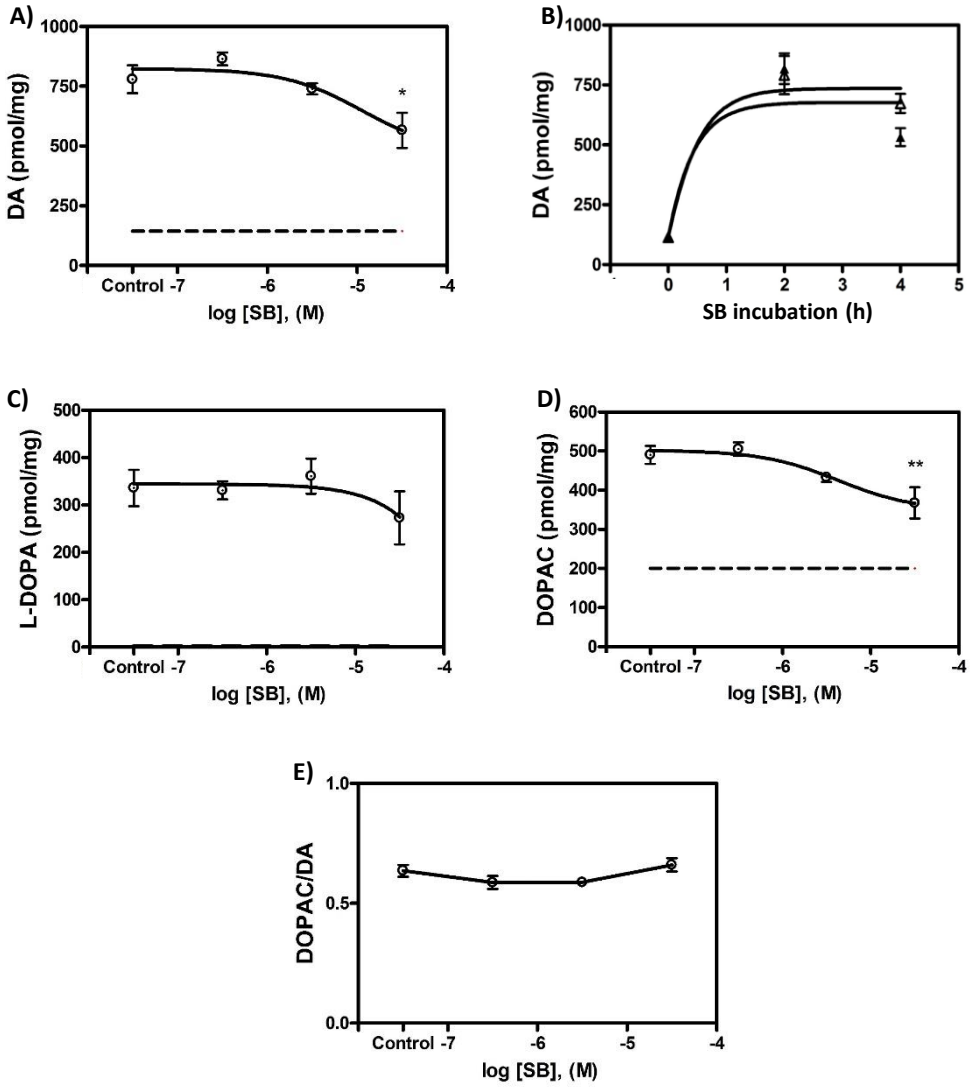
A)
DA (pmol/mg)
1000
750
500
250
0
Control -7
-6
-5
-4
log [SB], (M)
*
B)
DA (pmol/mg)
1000
750
500
250
0
0
1
2
3
4
5
SB incubation (h)
C)
L-DOPA (pmol/mg)
500
400
300
200
100
0
Control -7
-6
-5
-4
log [SB], (M)
D)
DOPAC (pmol/mg)
600
500
400
300
200
100
0
Control -7
-6
-5
-4
log [SB], (M)
**
E)
DOPAC/DA
1.0
0.5
0.0
Control -7
-6
-5
-4
log [SB], (M)

Figure 4

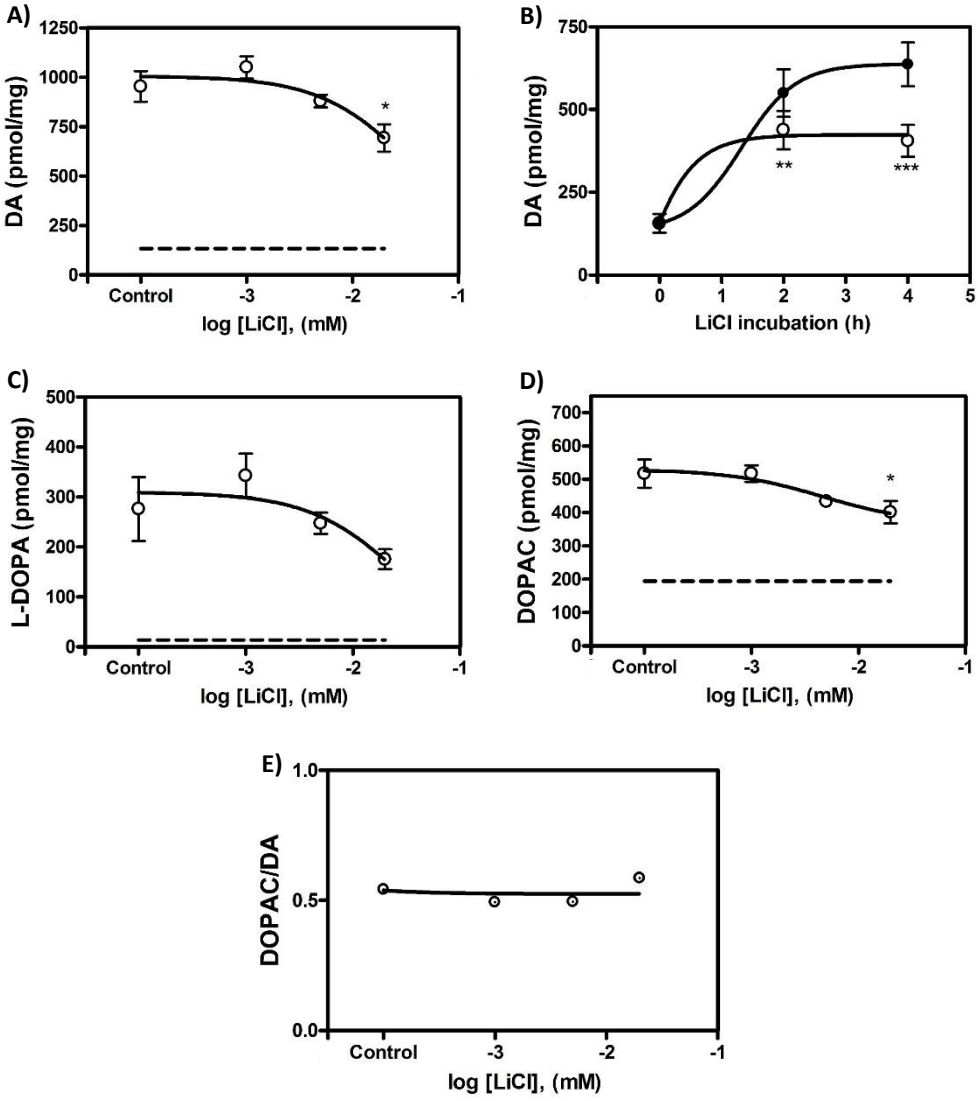
A)
DA (pmol/mg)
1250
1000
750
500
250
0
Control
-3
-2
-1
log [LiCl], (mM)
*
B)
DA (pmol/mg)
750
500
250
0
0
1
2
3
4
5
LiCl incubation (h)
**
***
C)
L-DOPA (pmol/mg)
500
400
300
200
100
0
Control
-3
-2
-1
log [LiCl], (mM)
D)
DOPAC (pmol/mg)
700
600
500
400
300
200
100
0
Control
-3
-2
-1
log [LiCl], (mM)
*
E)
DOPAC/DA
1.0
0.5
0.0
Control
-3
-2
-1
log [LiCl], (mM)

Figure 5

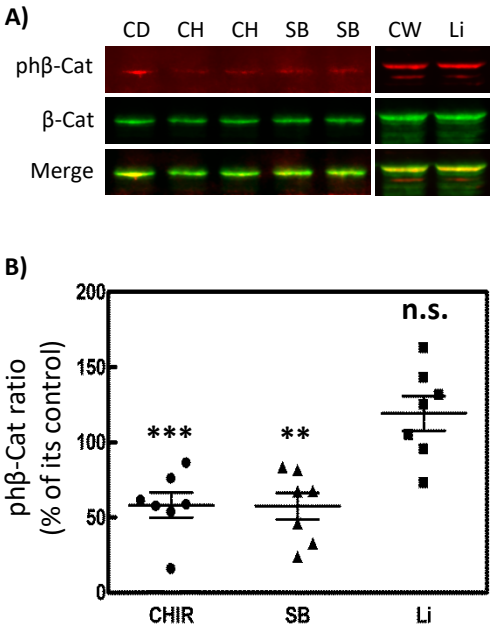
A)
CD
CH
CH
SB
SB
CW
Li
phβ-Cat
β-Cat
Merge
B)
phβ-Cat ratio
(% of its control)
200
150
100
50
0
***
**
n.s.
CHIR
SB
Li

Figure 6

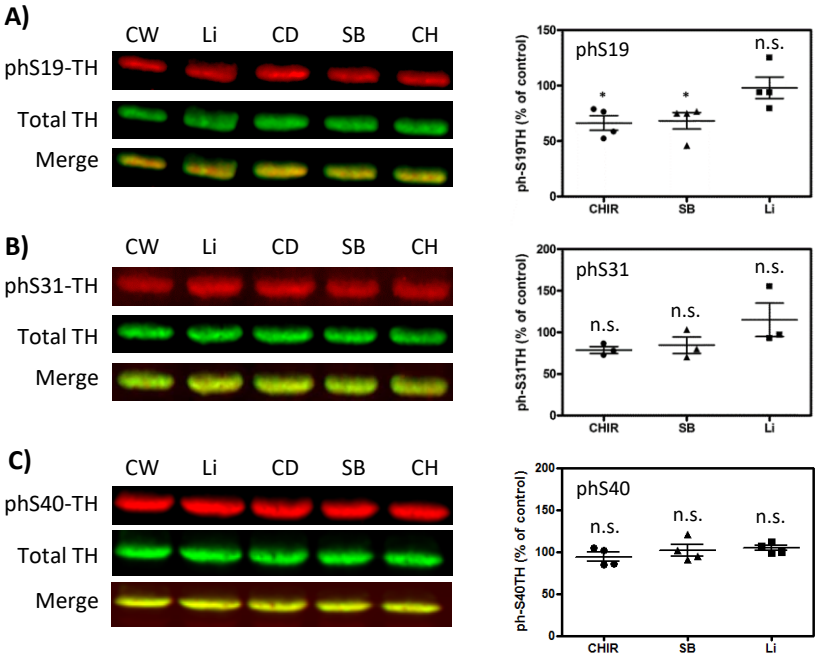
A)
CW
Li
CD
SB
CH
phS19-TH
Total TH
Merge
phS19
n.s.
ph-S19TH (% of control)
150
100
50
0
CHIR
SB
Li
B)
CW
Li
CD
SB
CH
phS31-TH
Total TH
Merge
phS31
n.s.
n.s.
n.s.
ph-S31TH (% of control)
200
150
100
50
0
CHIR
SB
Li
C)
CW
Li
CD
SB
CH
phS40-TH
Total TH
Merge
phS40
n.s.
n.s.
n.s.
ph-S40TH (% of control)
200
150
100
50
0
CHIR
SB
Li

Figure 7

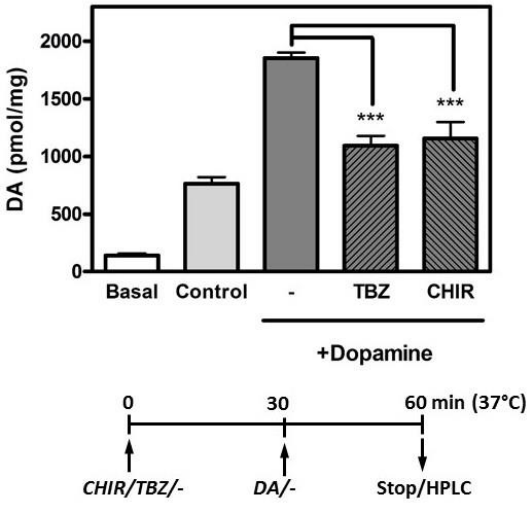
DA (pmol/mg)
2000
1500
1000
500
0
***
***
Basal
Control
-
TBZ
CHIR
+Dopamine
0
30
60 min (37°C)
CHIR/TBZ/-
DA/-
Stop/HPLC